Applied Thermal Engineering 180 (2020) 115853

Contents lists available at ScienceDirect

Applied Thermal Engineering

journal homepage: www.elsevier.com/locate/apthermeng

Distributed thermal management system for downhole electronics at high temperature

Wei Lan[a], Jiawei Zhang[b], Jiale Peng[a], Yiming Ma[a], Shuling Zhou[a], Xiaobing Luo[a,*]

[a] State Key Laboratory of Coal Combustion, School of Energy and Power Engineering, Huazhong University of Science and Technology, Wuhan 430074, China
[b] Well-Tech Research Institute of China Oilfield Service Limited, Beijing 101149, China

HIGHLIGHTS

- A distributed thermal management system was proposed for the logging tool.
- Complicated thermal system with nonlinear phase change process was simulated.
- The simulation was verified by the experiment.

ARTICLE INFO

Keywords:
Logging tool
High temperature
Distributed thermal management system
Phase change materials
Heat storage

ABSTRACT

The logging tools, which are widely utilized to detect the underground petroleum resources, are usually exposed to the high-temperature environment. Conventional thermal management system (CTMS) generally utilizes the vacuum flask for high-temperature insulation and phase change materials (PCMs) for centralized heat storage. As the heat sources increase and the skeleton becomes longer, the thermal performance of CTMS declines due to the increasing thermal resistance between heat sources and PCMs. To tackle this issue, a distributed thermal management system (DTMS) is proposed for the long-skeleton and multi-heat-source logging tools by arranging PCMs dispersedly in the skeleton. Numerical simulations are conducted to compare the performance of DTMS and CTMS. It is showed that the maximum temperature of DTMS decreases by 68 °C compared with CTMS, and the heat storage of PCMs in DTMS is 3.5 times higher than that in CTMS. Furthermore, the simulation results are validated by experimentally investigating the thermal performance of the logging tool with DTMS, and good agreement between the simulation and experiment is reached with the maximum relative error lower than 10%. DTMS is more practical for the realistic logging tools than CTMS, which may contribute to the development of the oil and gas detection in deeper and hotter wells.

1. Introduction

With the increasing demand for petroleum resources around the world, deeper and hotter wells are becoming more economical and attractive [1–4]. Logging tools are widely utilized in the oil and gas industry to accelerate the oil exploitation by measuring downhole environmental parameters including g pressure, temperature and viscosity [5]. After the drilling process, the wire-line logging tool is lowered into the well and then detects the distribution of petroleum resources. In general, the wire-line logging tool has to stay in the downhole for a couple of hours [6]. According to researches on the geosphere, a typical geothermal temperature rises 1–9 °C per 100 m as the well goes deeper, which reveals that the temperature of the wellbore would exceed 200 °C over a certain depth [7]. Actually, hundreds of high-pressure, high-temperature (HPHT) wells were discovered all around the world, where massive petroleum resources are stored [8,9]. In order to detect the HPHT wells, the electronics inside the logging tool have to endure wellbore temperature over 200 °C for several hours. However, most of the standard electronic components are unable to bear such a harsh environment, as the high temperature will lead to a decline of reliability or even complete failure of the electronics [10]. One of the possible solutions is to adopt the customized electronic components, which can survive at the surrounding temperature exceeding 200 °C. However, the usage of high-temperature electronics is uneconomic on account of their complex fabrication techniques [11–15].

In comparison with expensive high-temperature electronics, the thermal management system for downhole electronics is a more economical option. Several kinds of thermal management methods,

* Corresponding author.
E-mail address: luoxb@hust.edu.cn (X. Luo).

https://doi.org/10.1016/j.applthermaleng.2020.115853
Received 10 April 2020; Accepted 2 August 2020
Available online 09 August 2020
1359-4311/

including active cooling techniques and passive cooling techniques, have been applied successfully in the logging tools. Despite an outstanding cooling effect, active cooling techniques usually make the system complicated and unreliable due to a requirement of extra power input, other moving components and cooling liquid. Therefore, some active cooling techniques, such as thermoelectric cooling [16–19], sorption cooling [20,21], vapor compression cycle [22–24] and liquid cooling [25,26], are not recommended for the wire-line logging tool. In contrary to active thermal management techniques, passive thermal management techniques are more integrated and reliable. The conventional passive thermal management system (CTMS) usually contains the skeleton, electronic components, PCMs, insulators and a vacuum flask. Among them, the vacuum flask is utilized as a shell to protect the internal components from the high-temperature environment. The thermal insulators are placed at both ends of the vacuum flask to insulate the heat leakage from the opening. One or two pieces of PCMs located at the end of the skeleton are employed for centralized heat storage [27,28]. Besides, the electronic components are mounted on the skeleton. The temperature control effect on the electronic components is significant in CTMS, and it is perfect for the logging tool with few heat sources [29–31]. However, the industrial logging tool usually contains multiple electronic components and a long skeleton. The electronic components in the middle of the skeleton are away from the PCMs, and the thermal resistance between them increases as the distance between PCMs and heat sources becomes longer. Hence the heat generated by the electronic components in the middle is hard to be absorbed by the PCMs, which would lead to heat accumulation. As a consequence, due to the local overheating, the temperature control effect of CTMS deteriorates severely and the heat storage capacity of the PCM is difficult to be fully utilized. Therefore, the CTMS is incapable of satisfying the temperature control requirements of the long-skeleton and multi-heat-source logging tool, in which case an innovative thermal management system is needed.

In this work, a distributed thermal management system (DTMS) is proposed for the long-skeleton, multi-heat-source logging tool with the aim of reducing the thermal resistance between heat sources and PCMs. To illustrate the advantages of DTMS, the thermal performance of CTMS and DTMS was simulated using the finite element method, and the temperature as well as the utilization of PCMs is compared. Furthermore, the temperature experiment of the logging tool with DTMS was conducted to verify the simulation results.

2. Problem statement

Fig. 1(a) shows the structure of the logging tool with CTMS. It is based on a realistic instrument called nuclear magnetic resonance logging tool. It can be seen that the vacuum flask is utilized as a shell to protect the inner electronic components from the high-temperature environment. However, the heat leakage still intrudes into the vacuum flask through the opening at both ends. Hence two thermal insulators are placed at both ends of the vacuum flask, as a means to prevent the heat flow from entering the thermos. The skeleton is between two insulators where 14 pieces of heat sources are mounted. The heat power of the electronic components is listed in Table 1, and the total heat power is up to 90 W. It is noteworthy that the logging tool with CTMS only utilizes one piece of PCMs for centralized heat storage, which is adjacent to the insulator 1. As the distance between heat sources and PCMs becomes longer, the thermal resistance increases. As a result, the heat generated by the remote electronic components is hardly absorbed by the PCMs, thus the temperature control effect on the remote electronic components declines. To tackle this issue, a distributed passive thermal management system is proposed for the long-skeleton and multi-heat-source logging tool, as shown in Fig. 1(b). The PCMs are separated into six small parts, and then distributed to the skeleton. Each heat source can store heat in the nearby PCMs, thus the thermal resistance between heat sources and PCMs decreases. In consequence, the quantity of heat storage in PCMs increases, and the temperature of the logging tool becomes lower and more uniform.

To make a fair comparison, the type of the PCMs and the total amount of PCMs in both thermal management systems are the same. Besides, the size of the skeleton in DTMS is equivalent to CTMS. Both thermal management systems are required to stay in the environment of 205 ˚C for 9 h.

3. Methods

3.1. Simulation

In this section, we adopted the finite element method to simulate the thermal performance of CTMS and DTMS. To simplify the simulation, several reasonable assumptions were presented as follows:

1) Heat convection and radiation inside the vacuum flask is ignored.
2) The contact thermal resistance is ignored.
3) The electronic components are set as uniform volume heat sources.
4) The vacuum layer is equivalent to a solid layer with low thermal conductivity.

Based on the above assumptions, the simulation of the logging tool is simplified to a transient heat transfer problem, and it is governed by the heat-conduction equation [32]:

$$\rho c\frac{\partial T}{\partial t} = \nabla\cdot(\lambda\nabla T) + q \tag{1}$$

where ρ is the density, c is the specific heat and λ is the thermal conductivity. q means the energy generated per unit volume.

Since the phase transition of PCMs is a non-linear process, independent equations for PCMs are necessary. Eq. (2)-Eq. (5) are used to describe this non-linear phenomenon. During the melting process, the density of PCMs would change with the volume fraction of molten PCMs. Besides, the latent heat would seriously influence the heat storage capability of PCMs. Here, we adopt the effective heat capacity methods to solve the problem [33–35].

$$\rho_{PCM} = \theta\cdot\rho_{PCM.s} + (1-\theta)\cdot\rho_{PCM.l} \tag{2}$$

$$c_{PCM} = \frac{1}{\rho_{PCM}}[\theta\cdot\rho_{PCM.s}\cdot c_{PCM.s} + (1-\theta)\cdot\rho_{PCM.l}\cdot c_{PCM.l}] + L\frac{\partial\alpha_m}{\partial T} \tag{3}$$

$$\theta(T) = \begin{cases} 1 & T \leqslant T_m \\ \frac{V_{PCM.s}}{V_{PCM.s}+V_{PCM.l}} & T_m < T < T_m + \Delta T \\ 0 & T_m + \Delta T \leqslant T \end{cases} \tag{4}$$

$$\alpha_m = \frac{1}{2}\frac{(1-\theta)\cdot\rho_{PCM.l} - \theta\cdot\rho_{PCM.s}}{(1-\theta)\cdot\rho_{PCM.l} + \theta\cdot\rho_{PCM.s}} \tag{5}$$

where ρ_{PCM}, $\rho_{PCM.s}$, $\rho_{PCM.l}$ means the density of the PCMs, the density of the solid PCMs and the density of the molten PCMs, respectively. In addition, c_{PCM}, $c_{PCM.s}$, $c_{PCM.l}$ represents the heat capacity of the PCMs, the heat capacity of the solid PCMs and the heat capacity of the molten PCMs, respectively. T_m is the melting point of PCMs, Δ T means the phase transition interval and L means the latent heat of the PCMs. Moreover, θ is a piecewise function related to the melting point and indicates the volume fraction of solid PCMs. α_m means the phase transition mass fraction from solid phase to liquid phase.

Thermal convection occurs between the outer surface of the vacuum flask and the high-temperature environment. It could be assumed as a Cross-Flow-Over-Cylinders problem and described by Eq. (6)-Eq. (9) [36,37].

$$q_{out} = h(T_{fluid} - T) \tag{6}$$

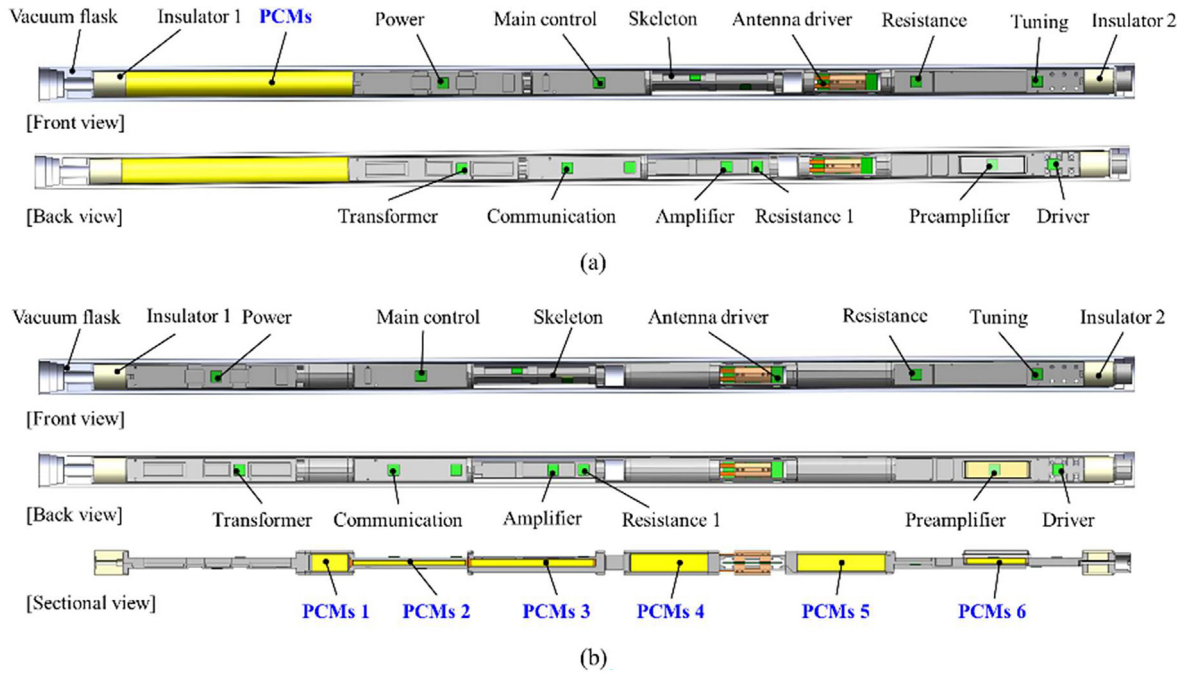

Fig. 1. Structure of the logging tool with (a) CTMS and (b) DTMS.

Table 1
Heat sources of the logging tool.

Component	Power (W)	Component	Power (W)
Power	7	Communication	2 × 2
Main control	2	Amplifier	3 × 3
Antenna driver	24	Resistance 1	14
Resistance	15	Preamplifier	1
Tuning	4	Driver	3
Transformer	7		
Total power			90

$$h = \frac{\lambda_{fluid}}{D}\left\{0.3 + \frac{0.62\mathrm{Re}^{1/2}\mathrm{Pr}^{1/3}}{[1 + (0.4/\mathrm{Pr})^{2/3}]^{1/4}}\left[1 + \left(\frac{\mathrm{Re}}{282000}\right)^{5/8}\right]^{4/5}\right\} \quad (7)$$

$$\mathrm{Re} = u_{fluid} D/\nu_{fluid} \quad (8)$$

$$\mathrm{Pr} = \nu_{fluid}/a_{fluid} \quad (9)$$

where q_{out} means the heat flow from the environment to the vacuum flask, h is called the convection heat-transfer coefficient and calculated by Eq. (9). T_{fluid}, λ_{fluid}, u_{fluid}, ν_{fluid} *and* a_{fluid} represent the temperature, the thermal conductivity, the velocity, the kinematic viscosity and the thermal diffusivity of the environmental fluid, respectively. D is the diameter of the vacuum flask.

The temperature distribution of the logging tool was simulated by the commercial finite element software. Firstly, the governing equations mentioned above were added into the CFD solver. Then the three-dimensional geometry model was imported, and the unstructured grids were generated. The computational domain includes the air domain, which exists in the gap between the inner side of the vacuum flask and the skeleton. Afterward, the materials of the components were defined, and the thermal properties are shown in Table 2. It is noteworthy that the melting point of PCMs (RT-70, RUBITHERM, Germany) is 70.84 °C and the latent heat reaches 258.6 kJ·kg^{-1}, which are measured by the DSC test. Besides, the vacuum layer was assumed as a solid layer with an equivalent thermal conductivity of 0.0002 W·m^{-1}·K^{-1} according to the parameters given by the manufacturer. Next, some essential boundary conditions were established. The initial temperature of all domains was set to 26 °C, and the environment temperature was set to 205 °C. Furthermore, the heat power of the heat sources was set according to Table 1. In the end, the case was calculated for 9 h with the time step of 10 min.

Table 2
Materials and thermal properties of logging tool components.

Component	Material	Thermal conductivity (W·m^{-1}·K^{-1})	Density (kg·m^{-3})	Heat capacity (J·kg^{-1}·K^{-1})
Vacuum flask	TC-11	7.5	4480	550
Vacuum layer	Composite	0.0002	100	1200
Skeleton	Aluminum Alloy	130	2810	960
Simulated heat sources	Ceramic	20	2145	750
PCMs	Paraffin	880(s)/770(l)	0.2	2000
PCMs container	304	7930	16.3	500
Heat sink	Copper	400	8700	385
Insulator 1	PTFE	0.25	2200	1000
Insulator 2	Aerogel blanket	0.025	250	502.3

3.2. Experiment

To verify the simulation, the temperature experiment of the logging tool with DTMS was conducted. As shown in Fig. 2(a), a prototype of the logging tool with DTMS was fabricated on a scale of one to one, and its size was ∅ 91 mm × 3820 mm. It was assembled by several components including six pieces of PCMs. Among the PCMs modules, three pieces were the parts of the skeleton, while the others were embedded into the skeleton. Fig. 2(b) showed all of the PCMs packaging modules.

After the fabrication of the prototype, two preparations were required for the logging tool temperature experiment. First, several pieces of ceramic heating elements (40 mm × 40 mm × 2 mm, heat power customization, Beijing youpu science and Technology Centre) were utilized as the simulated heat sources, and they were attached to the skeleton by thermal interface materials (2 W·m^{-1}·K^{-1}, XK-P20S20, GLPOLY). The layout of the simulated heat sources was the same as Fig. 1(b). Second, thermocouples (K-Type, 2 × 0.3 mm) were fixed on

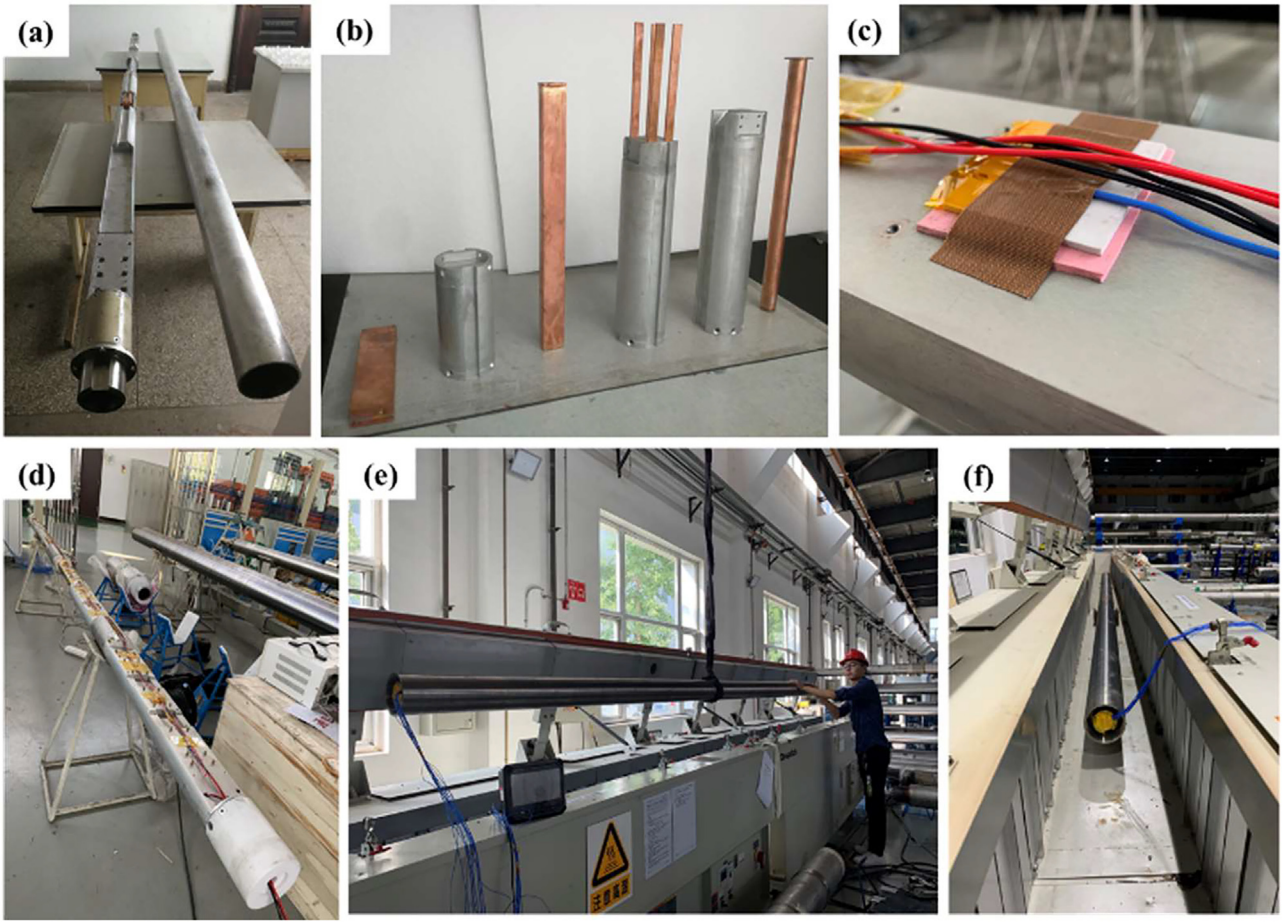

Fig. 2. (a) Prototype of the logging tool with DTMS, (b) PCMs packaging modules in DTMS, (c) Simulated heat source and thermocouple, (d) Prototype of DTMS with simulated heat sources and thermocouples, (e) Experimental site, (f) Prototype in the oven.

13 temperature measuring points, including the outer surface of the vacuum flask, insulators, several simulated heat sources and the PCMs modules. Fig. 2(c) showed the simulated heat source and the thermocouple. The white plate implied the ceramic heating elements, and the pink pad was the thermal silicon pad. The blue line meant the thermocouple, which was stuck on the surface of the heating elements. Fig. 2(d) showed the full view of the prototype with simulated heat sources and thermocouples. The red–black power supply cord entered from one end, and the thermocouple wires entered from the other end.

Afterward, the prototype with simulated heat sources and thermocouples was stuffed in the vacuum flask (YJPST128x4031/92.5, Xi'an Yufeng Electronic Engineering Company, China). Then the prototype and the vacuum flask were lifted into the oven (operating range 51 °C–260 °C, PTC1-40, Despatch), as shown in Fig. 2(e) and Fig. 2(f). The temperature of the oven was set to 205 °C, and the experiment lasted for 9 h. All of the temperature data was recorded by a data acquisition instrument (Accuracy 0.2%FS ± 1D, MIK-6000F, Hangzhou Meacon Automation Technology Company) with a sampling period of one second.

4. Result and discussion

4.1. Temperature performance in DTMS and CTMS

To distinguish the differences between DTMS and CTMS, the temperature analysis is proposed. Fig. 3(a) presents the temperature distribution of the logging tool with CTMS (left) and DTMS (right) at 9 h. It is obvious that the maximum temperature of CTMS is higher than DTMS. And the temperature almost linearly increases with the distance to PCMs except antenna driver due to its highest heat power. On the contrary, DTMS displays a lower and more uniform temperature distribution on account of the reduction of thermal resistance between heat sources and PCMs. Fig. 3(b) quantitatively compares the temperature of several typical heat sources. The bar chart shows a similar trend to Fig. 3(a), and the temperature of the selected heat sources in DTMS are apparently lower than that in CTMS. The maximum temperature of CTMS reaches as high as 214 °C, far exceeding the operating temperature of the electronic components. By contrast, the maximum temperature sharply drops to 146 °C in the logging tool managed by DTMS, which is still within the allowable temperature range of the electronic components. The mean temperature drop of these five heat sources is up to 60.9 °C. According to the analysis above, it can be concluded that DTMS possesses a better temperature control performance than CTMS.

Fig. 3(a) and Fig. 3(b) is merely focused on the temperature distribution of the logging tool at the end of the time, while Fig. 3(c) and Fig. 3(d) display the time-varying process of temperature. As can be seen from the graphs below, the curves of the heat sources' temperature in CTMS rise at a roughly constant slope owing to the insignificant effects of PCMs. Similarly, the curves of temperature in DTMS lift sharply at first. However, when the temperature rises slightly above the PCMs melting point (70.84 °C), the PCMs maintain at a constant temperature owing to the large latent heat, thus effectively restrain the rising rate of heat sources' temperature. As a result, the temperature of electronic components in DTMS is notably lower than the temperature in CTMS eventually.

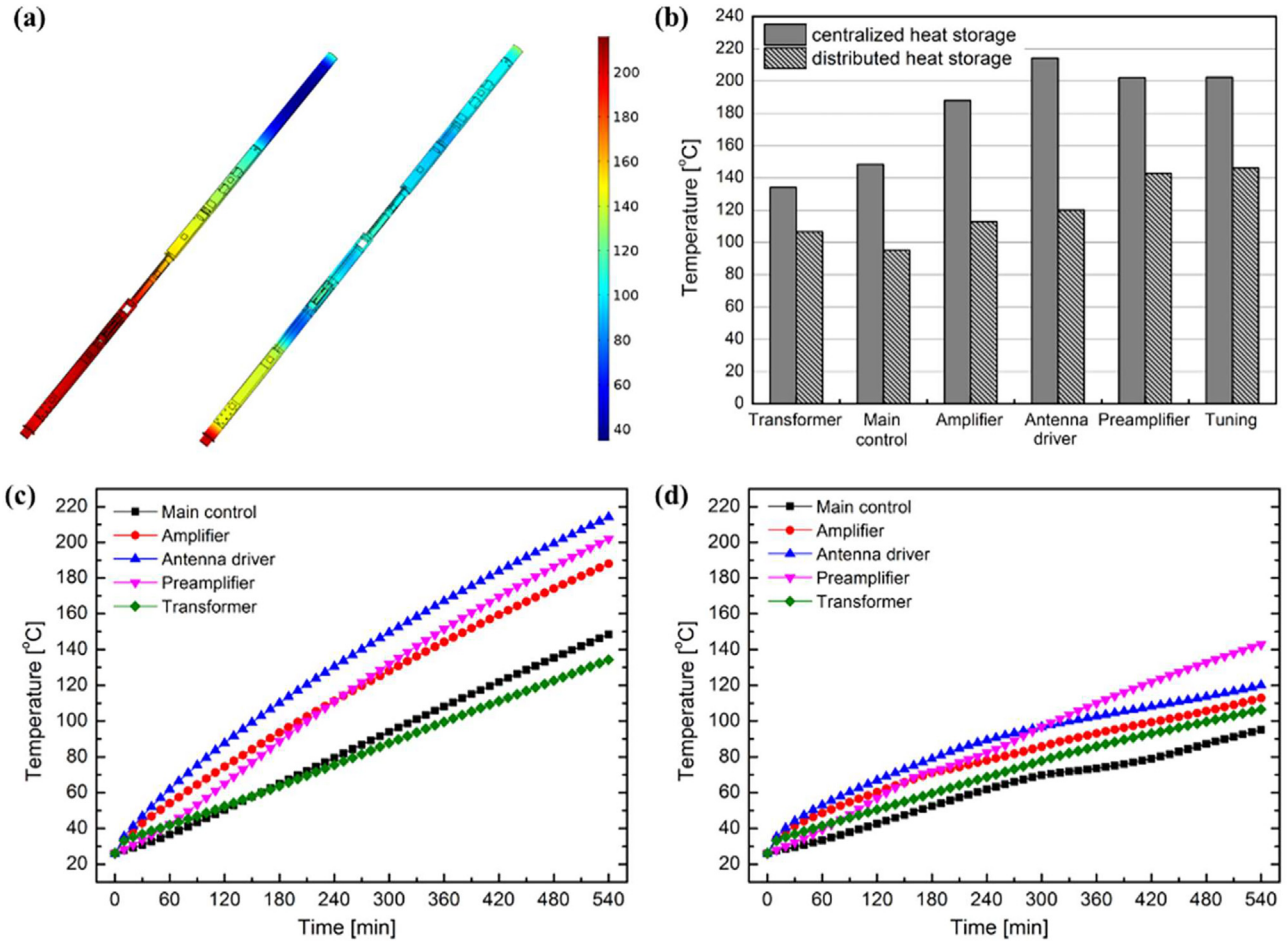

Fig. 3. (a) Temperature contour of logging tool with CTMS (left) and DTMS (right) at 9 h, (b) Comparison of heat sources temperature between CTMS and DTMS, (c) Curves of heat sources temperature versus time in CTMS, (d) Curves of heat sources' temperature versus time in DTMS.

4.2. The utilization of PCMs in DTMS and CTMS

In this section, the performances of PCMs in DTMS and CTMS during the heating up process are investigated. Fig. 4(a) presents the contour of PCMs' phase transition process in CTMS, where 0 represents the solid PCMs while 1 represents the PCMs that have been totally molten. As shown in Fig. 4(a), the phase transition doesn't occur within the first five hours since the maximum temperature of PCMs doesn't reach the melting point. After 6 h, the right side of PCMs begins to melt, whereas the center and the left side are still unmolten. It can be explained by two reasons. For one thing, PCMs are heated by the metal skeleton, thus the surfaces of PCMs reach the highest temperature and melt firstly; For another, a notable thermal resistance exists inside the PCMs leading to the non-uniform temperature distribution. At the end of 9 h, only the left side of the PCMs are melting, which implies that a large amount of heat storage capacity of PCMs is waste.

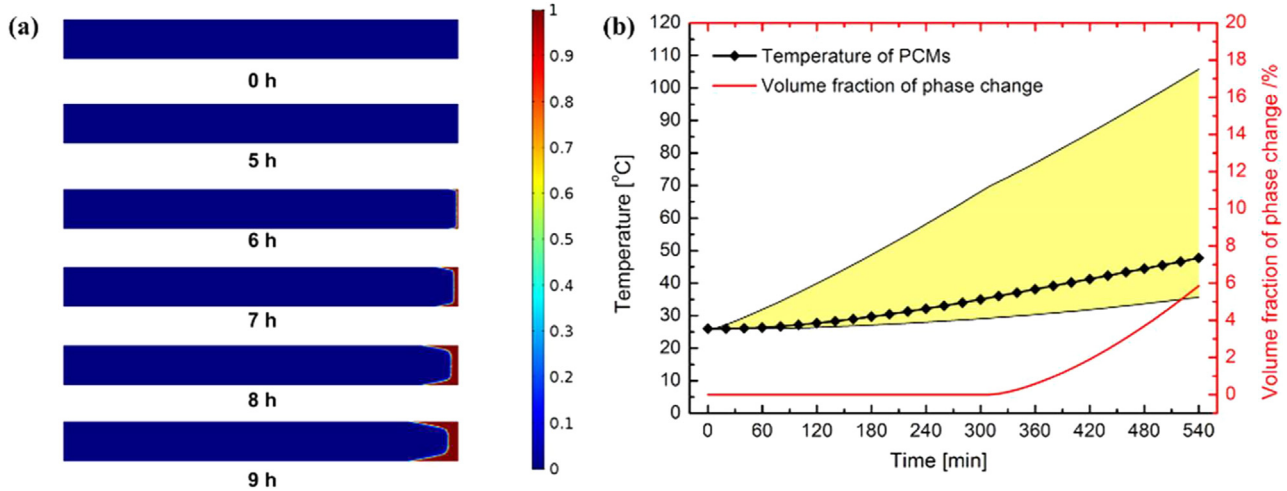

Fig. 4. (a) Contour of PCMs' phase transition process in CTMS, (b) Curves of PCMs' temperature and phase change percentage versus time in CTMS.

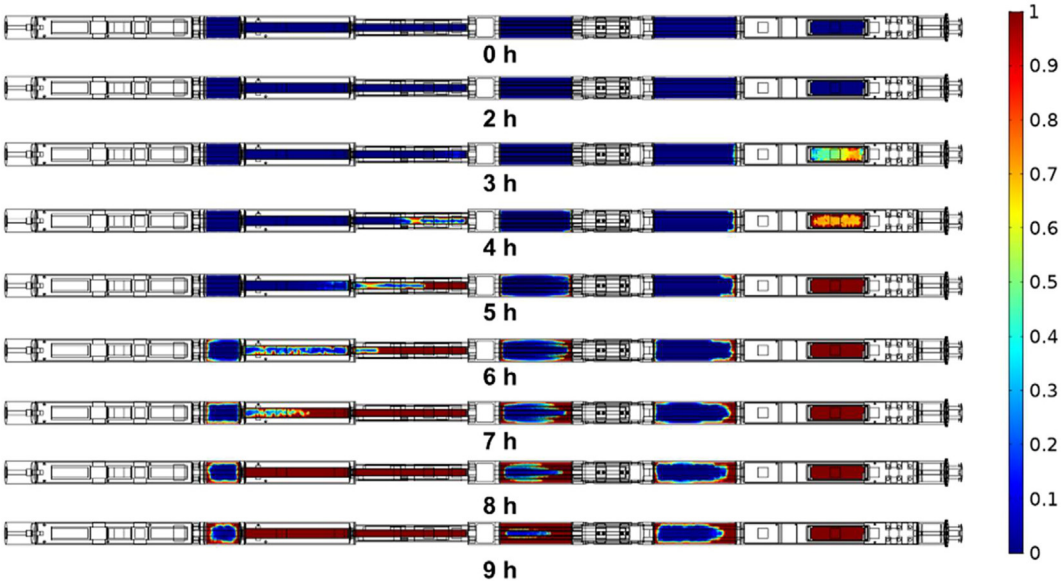

Fig. 5. Contour of PCMs' phase transition process in DTMS.

Fig. 4(b) presents a curve of PCMs' average body temperature along with a curve of phase change percentage versus time in CTMS. The yellow zone means the temperature range of the PCMs, and the edges of the yellow area imply the maximum temperature and minimum temperature of PCMs. At the end of 9 h, the maximum temperature of PCMs is 106 °C, while the minimum temperature is 35 °C. The vast difference between maximum temperature and minimum temperature implies the significant thermal resistance inside the PCMs. Besides, the curve of phase change percentage in CTMS indicates that the phase change process begins at around 6 h, and the final utilization rate of the latent heat reaches up to 6%.

The contour of PCMs' phase transition process in DTMS is as shown in Fig. 5. Six pieces of PCMs behave differently. For instance, owing to a massive amount of heat leakage from the opening of the vacuum flask, PCMs 6 melts at first and completes the phase transition process beyond other PCMs. At the end of the operation time, PCMs 2, PCMs 3 and PCMs 6 accomplish the phase transformation revealing that the latent heat of these PCMs is fully utilized. Though the rest of the PCMs haven't melted totally, they still absorb a large amount of heat, as shown in Table 3. The total amount of PCMs heat storage in DTMS is 961.10 kJ, which is 3.5 times larger than that in CTMS.

Further analysis shows a quantitative description of the phase-change volume fraction of each PCMs versus time in DTMS, as shown in Fig. 6. The latent heat utilization rates of PCMs 1, PCMs 4 and PCMs 5 are 70%, 92.4%, and 55%, respectively. The rest of the PCMs reach up to 100% utilization rate of latent heat; hence the total PCMs make 77.6% use of latent heat during the operation time. Nevertheless, the utilization rate of latent heat in DTMS is still far higher than that in CTMS. As a result, DTMS makes tremendous progress in temperature control performance, which has been discussed in the last section.

4.3. Experimental validation

Fig. 7 shows the experimental temperature curves of the measuring points versus time. Since the number of the experimental curves is up to 13, it wouldn't be easy to find out each curve if all the curves are displayed in one figure. Therefore, the experimental results are divided into three figures by category. From Fig. 7(a), the environment temperature rises sharply at first and then maintains at 205 °C after 60 min. The temperature curves of several heat sources are also investigated here. And the temperature of them is below 150 °C during the heating-up process, which is still within the electronic operating temperature range. Among all of the heat sources, the temperature of the tuning board is the highest owing to the great influence of the heat leakage from high-temperature environment. Fig. 7(b) shows the experimental temperature curves of insulators and PCMs. There are two apparent turning points and a flat zone in three curves of PCMs, indicating that the PCMs pass through the phase transition process during the

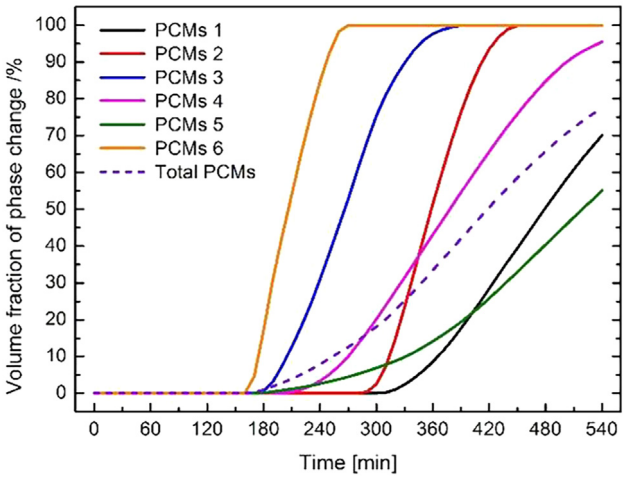

Fig. 6. Curves of PCMs' phase change volume fraction versus time in DTMS.

Table 3
Heat storage of PCMs in DTMS and CTMS.

	PCMs 1	PCMs 2	PCMs 3	PCMs 4	PCMs 5	PCMs 6	Total
DTMS	152.60 kJ	78.02 kJ	74.46 kJ	369.33 kJ	204.36 kJ	82.32 kJ	961.10 kJ
CTMS	\	\	\	\	\	\	213.93 kJ
Heat storage difference							747.17 kJ

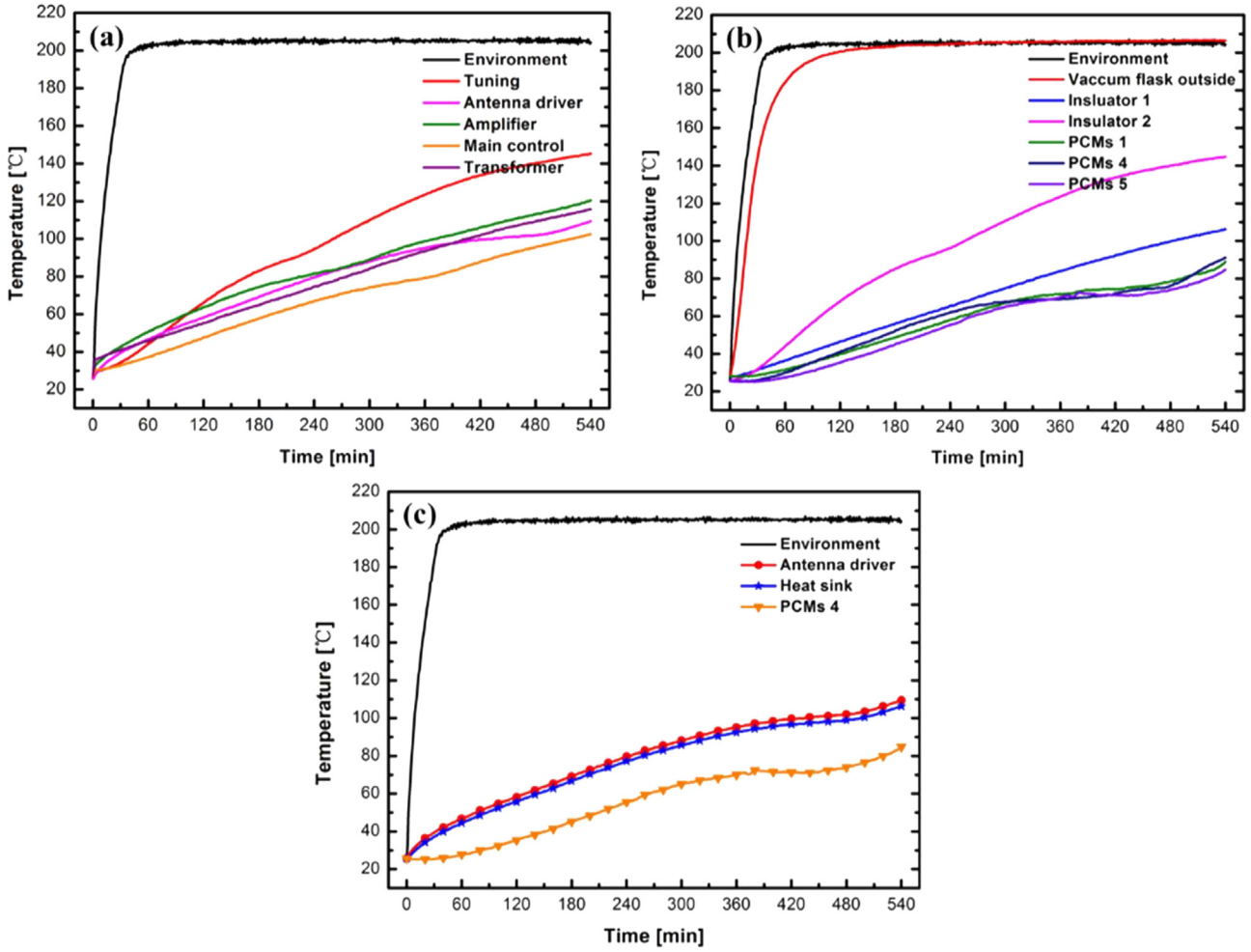

Fig. 7. (a) Experimental temperature curves of heat sources versus time, (b) Experimental temperature curves of insulators and PCMs, (c) Experimental temperature curves of antenna driver under the control of PCMs 4.

experiment. Compared to the insulator 1, the temperature of the insulator 2 is much higher as a consequence of the severe heat leakage from the large opening of the vacuum flask. Fig. 7(c) selects three representative curves to illustrate the temperature control effect of the PCMs on the heat sources. It is shown that PCMs 4 maintains at the melting point from 360 min to 480 min, and the temperature curves of the antenna driver and the heat sink are obviously restrained similar to the curve of PCMs 4. The result confirms the temperature control effect of the PCMs on the heat sources.

To verify the simulation, the temperature of five measuring points between experiment and simulation are compared in Fig. 8. The curves represent the temperature results of the simulation, while the scatter points represent the experimental results. Though the curves are unable to match the scatter points perfectly, the trend of the simulation results is similar to the experimental results. The curves and the scatter plots become mild during the phase change process, especially for PCMs 1. To quantitatively compared the experiment data and simulation data, several statistics are utilized to judge the agreement between simulation results and experimental results, including relative error (RE), root mean square error (RMSE), and correlation coefficient (r). Among them, RE is utilized to measure the temperature error between simulation and experiment at a specific moment, while RMSE is used to assess the temperature error through the whole heating-up process. Besides, r is utilized to measure the strength of a linear relationship between the simulation data and experimental data. First, the simulation temperature and experimental temperature at the end of time are compared, the maximum RE of all the measuring points is lower than 10% and the

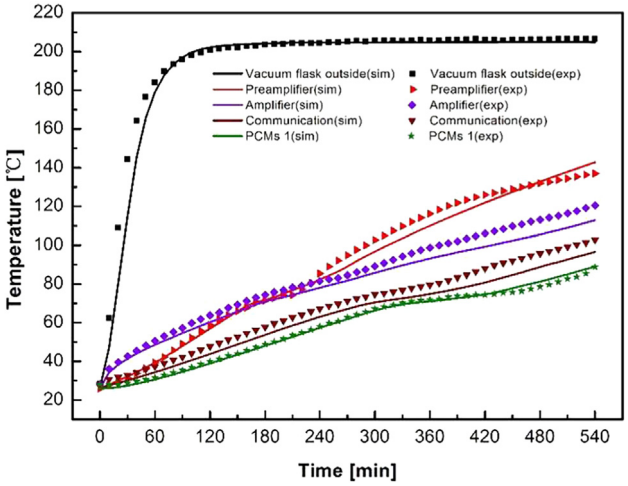

Fig. 8. Comparison of temperature curves between experiment and simulation.

average RE is below 5%. Then the agreement between the data sets of simulation and experiment is further investigated. The results show that RMSE between two data sets is within 9 °C, and r between the simulation results and the experimental results is larger than 0.99, which implies that the trend of the simulation data is highly consistent with the experimental data. In summary, the analyses above indicate that the simulation of the logging tool is reasonable, hence the discussions about

the thermal performance of the logging tool with DTMS and CTMS in Sections 4.1 and 4.2 are convincing.

Furthermore, the reasons behind the deviation between the experiment and simulation are studied. The deviation is mainly caused by the assumptions in the simulation. Firstly, the neglect of the heat convection and radiation inside the flask attenuates the heat transfer between the vacuum flask and the skeleton, which would reduce the simulation temperature of the skeleton and the heat sources. Secondly, owing to the disregard of the contact thermal resistance, the thermal resistance between the adjacent components would decline, leading to the enhancement of the heat transfer between heat sources and PCMs. Hence the temperature of PCMs would be lower in the simulation. Thirdly, the vacuum layer is equivalent to a solid layer with low thermal conductivity, regardless of the radiation between the radiation shields inner the vacuum layer. Although an equivalent thermal conductivity is given by the manufacturer, it may still cause a deviation.

5. Conclusions

A distributed thermal management system (DTMS) is proposed for the long-skeleton and multi-heat-source logging tool by dispersing the PCMs into the skeleton to decrease the thermal resistance between heat sources and PCMs. The finite element method is utilized to simulate the performance of CTMS and DTMS. Then the experiment of the logging tool with DTMS is conducted to verify the simulation results. The simulation results show that the temperature of DTMS is lower and more uniform than that of CTMS, and the maximum temperature drops from 214 ˚C to 146 ˚C. Besides, the utilization rate of latent heat in DTMS is up to 77.6%, which is far higher than 6% in CTMS, corresponding to the heat storage enhancement of 3.5 times. Further, the experimental results show that the temperature of all components is lower than 150 ˚C, which is still within the electronic operating temperature range. Besides, the maximum relative error between simulation results and experimental results is lower than 10%, and the correlation coefficient is larger than 0.99, demonstrating a good agreement between the simulation and experiment. In summary, DTMS possesses a better temperature control performance than CTMS for the long-skeleton and multi-heat-source logging tools, which may be beneficial to the oil and gas detection in deeper and hotter wells.

Declaration of Competing Interest

The authors declare that they have no known competing financial interests or personal relationships that could have appeared to influence the work reported in this paper.

Acknowledgement

The authors would like to acknowledge the financial support by National Natural Science Foundation of China (51625601, 51606074), the Ministry of Science and Technology of the Peoples Republic of China (Project No. 2017YFE0100600), the financial support from Creative Research Groups Funding of Hubei Province (2018CFA001).

Appendix A. Supplementary data

Supplementary data to this article can be found online at https://doi.org/10.1016/j.applthermaleng.2020.115853.

References

[1] S. Soprani, A.J. Nørgaard, C. Nesgaard, K. Engelbrecht, Design and Testing of a Heat Transfer Sensor for Well Exploration Tools, Appl. Therm. Eng. 141 (2018) 887–897.
[2] L.J. Bernard, S. Dyer, A. Harrison, M. Arena, W. Luckett, Testing Oilfield Technologies for Wellsite Operations, Oilfield Rev. 17 (4) (2005) 58–67.
[3] T. Baird, T. Fields, R. Drummond, High-Pressure, High-Temperature Well Logging, Perforating and Testing, Oilfield Rev. 10 (2) (1998) 50–67.
[4] H. Zhang, H. Liu, S. Wu, J. Sun, C. Yang, Y. Xie, C. Chen, J. Gao, J. Wang, Pre-Drilling Prediction Techniques On the High-Temperature High-Pressure Hydrocarbon Reservoirs Offshore Hainan Island, China, J. Ocean U. China 17 (1) (2018) 72–82.
[5] J. Boyes, The Eyes of the Oil Industry, Electron. Power 27 (6) (1981) 484–488.
[6] A. Sinha, Y.K. Joshi, Downhole Electronics Cooling Using a Thermoelectric Device and Heat Exchanger Arrangement, J. Electron. Packaging 133 (4) (2011) pp. 041005–041005-12.
[7] N.J. Hyne, Nontechnical Guide to Petroleum Geology, Exploration, Drilling & Production, PennWell Corp, Tulsa, USA, 2001.
[8] I. Lunney, A. Duriez, T. Solbakk, M.B. Skaug, T. Brian, Harsh Environment Logging-while-Drilling Tools Enhance Well Performance in North Sea Hpht Wells, SPE Europec featured at 79th EAGE Conference and Exhibition, (2017).
[9] G. DeBruijn, C. Skeates, R. Greenaway, D. Harrison, M. Parris, S. James, F. Mueller, S. Ray, M. Riding, L. Temple, K. Wutherich, High-Pressure, High-Temperature Technologies, Oilfield Rev. 20 (3) (2008) 46–60.
[10] X. Luo, R. Hu, S. Liu, K. Wang, Heat and Fluid Flow in High-Power Led Packaging and Applications, Prog. Energ. Combust. 56 (2016) 1–32.
[11] J. Watson, G. Castro, A Review of High-Temperature Electronics Technology and Applications, J. Mater. Sci.: Mater. Electron. 26 (12) (2015) 9226–9235.
[12] E.H. Amalu, N.N. Ekere, R.S. Bhatti, High Temperature Electronics: R&D Challenges and Trends in Materials, Packaging and Interconnection Technology, in: International Conference on Adaptive Science & Technology, January 14-16, 2009, pp. 146–153.
[13] M.R. Werner, W.R. Fahrner, Review On Materials, Microsensors, Systems, and Devices for High-Temperature and Harsh-Environment Applications, Ieee T. Ind. Electron. 48 (2) (2001) 249–257.
[14] P.L. Dreike, D.M. Fleetwood, D.B. King, D.C. Sprauer, An Overview of High-Temperature Electronic Device Technologies and Potential Applications, IEEE T. Comp. Pack. Man. 17 (4) (2009) 594–609.
[15] V.K. Khanna, Extreme-Temperature and Harsh-Environment Electronics, Phys., Technol. Appl. (2017).
[16] S. Soprani, J.H.K. Haertel, B.S. Lazarov, O. Sigmund, K. Engelbrecht, A Design Approach for Integrating Thermoelectric Devices Using Topology Optimization, Appl. Energ. 176 (2016) 49–64.
[17] S. Soprani, K. Engelbrecht, A. Just Nørgaard, Active Cooling and Thermal Management of a Downhole Tool Electronics Section, International Institute of Refrigeration, Yokohama, Japan, August, 2015, pp. 16–22.
[18] R. Weerasinghe, T.P. Hughes, Thermal Management of Downhole Measuring Tools Using Thermoelectric Cooling; A Numerical and Experimental Investigation, 12th International Conference on Heat Transfer, Fluid Mechanics and Thermodynamics, Costa de Sol, Spain, July 11-13, 2016, pp. 1654–1659.
[19] J. Kähler, A. Stranz, A. Waag, E. Peiner, Thermoelectric Coolers with Sintered Silver Interconnects, J. Electron. Mater. 43 (6) (2014) 2397–2404.
[20] E. Pennewitz, T. Kruspe, S. Jung, M. Schilling, Evaluation of Sorbents at Elevated Temperatures for Downhole Application, MILANO, Chemical Engineering Transactions, 2012, pp. 1543–1548.
[21] E. Pennewitz, M. Schilling, T. Kruspe, S. Jung, A. Ruehs, Active cooling of downhole instrumentation for drilling in deep geothermal reservoirs, in: 2012 IEEE International Instrumentation and Measurement Technology Conference Proceedings, Graz, 2012, pp. 600–603.
[22] S. Verma, Q. Elias, Thermal Management of Electronics Used in Downhole Tools, SPE Annual Technical Conference and Exhibition, San Antonio, Texas, USA, October 8-10, 2012.
[23] G. Aaron, Active Cooling for Electronics in a Wireline Oil-Exploration Tool, Massachusetts Inst. Technol. (1996).
[24] W. Gao, K. Liu, H. Jia, D. Hong, X. Teng, Challenge of Temperature Control for Downhole Instruments in HTHP Reservoir, SPE Offshore Europe Conference and Exhibition, Aberdeen, (2019).
[25] J. Jakaboski, Innovative Thermal Management of Electronics Used in Oil Well Logging, Georgia Inst. Technol. (2004).
[26] R. Wu, Y. Fan, T. Hong, H. Zou, R. Hu, X. Luo, An immersed jet array impingement cooling device with distributed returns for direct body liquid cooling of high power electronics, Appl. Therm. Eng. 162 (2019) 114259.
[27] J. Pereira Da Cunha, P. Eames, Thermal Energy Storage for Low and Medium Temperature Applications Using Phase Change Materials – a Review, Appl. Energ. 177 (2016) 227–238.
[28] H. Nazir, M. Batool, O. Bolivar, J. Francisco, M. Isaza-Ruiz, X. Xu, et al., Recent developments in phase change materials for energy storage applications: A review, Int. J. Heat Mass Tran. 129 (2019) 491–523.
[29] B. Shang, Y. Ma, R. Hu, C. Yuan, J. Hu, X. Luo, Passive Thermal Management System for Downhole Electronics in Harsh Thermal Environments, Appl. Therm. Eng. 118 (2017) 593–599.
[30] Y.P. Ma, B.F. Shang, R. Hu, X.B. Luo, Thermal Management of Downhole Electronics Cooling in Oil & Gas Well Logging at High Temperature, in: 17th International Conference on Electronic Packaging Technology, NEW YORK, 2016, pp. 623–627.
[31] S. Rafie, Thermal Management of Downhole Oil & Gas Logging Sensors for Hthp Applications Using Nanoporous Materials, in: Proceedings of 2nd Energy Nanotechnology International Conference, Vol. 81, No. 2, Supplement, (2007) pp. S910–S931.
[32] J.P. Holman, Heat Transfer, CHINA MACHINE PRESS, Beijing, 2011.
[33] M. Iten, S. Liu, A. Shukla, Experimental Validation of an Air-Pcm Storage Unit Comparing the Effective Heat Capacity and Enthalpy Methods through Cfd Simulations, Energy 155 (2018) 495–503.

[34] Y. Zhang, Modified Computational Methods Using Effective Heat Capacity Model for the Thermal Evaluation of Pcm Outfitted Walls, Int. Commun. Heat Mass 108 (2019) 104278.
[35] H. Yang, Y. He, Solving Heat Transfer Problems with Phase Change Via Smoothed Effective Heat Capacity and Element-Free Galerkin Methods, Int. Commun. Heat Mass 37 (4) (2010) 385–392.
[36] S.W. Churchill, M. Bernstein, A Correlating Equation for Forced Convection From Gases and Liquids to a Circular Cylinder in Crossflow, J. Heat Transf. 99 (2) (1977) 300–306.
[37] M. Elsheniti, A. Kotb, O. Elsamni, Thermal performance of a heat-pipe evacuated-tube solar collector at high inlet temperatures, Appl. Therm. Eng. 154 (2019) 315–325.